Measuring Ripple and Dune Migration in Coprates Chasma, Valles Marineris: A Source to Sink Aeolian System on Mars?

Measuring Ripple and Dune Migration in Coprates Chasma, Valles Marineris: A Source to Sink Aeolian System on Mars?

S. J. Boazman[1,2], J.M. Davis[1], P. M. Grindrod[1], M. R. Balme[3], P.Vermeesch[2], T. Baird[2]

[1]Dept. of Earth Sciences, Natural History Museum, London, UK.

[2]Dept. of Earth Sciences, University College London, London, UK.

[3]Dept. of Physical Sciences, Open University, Milton Keynes, UK.

Corresponding author: Sarah Boazman (s.boazman@nhm.ac.uk)

Key Points:

- Dune brink and ripple migration in Coprates Chasma quantified for both short and long time periods for Earth years 2007-2014.
- Potential sources for the dune field evaluated using thermal inertia and mineralogy.
- Canyon topography may influence the local wind regime and thus the activity of bedforms.

This article has been accepted for publication and undergone full peer review but has not been through the copyediting, typesetting, pagination and proofreading process, which may lead to differences between this version and the Version of Record. Please cite this article as doi: 10.1029/2020JE006608.

Abstract

Active aeolian systems are present across the martian surface, with active dune fields commonly found in depressions such as craters and valleys. There are many dune fields within the equatorial region of Mars, including Valles Marineris, but the effects of topography on wind regimes and consequently dune migration in Valles Marineris is poorly understood. We investigated both the ripple and dune migration in a dune field in Coprates Chasma using High Resolution Science Experiment Images (HiRISE) and Context Camera (CTX) images. Migration rates of dune brinks and ripples were measured over varying time scales, between Earth years 2007-2014. The dunes here are some of the tallest on Mars, with heights of up to 182 m. The dune brinks are migrating eastwards at a rate of 0.1-0.3 m/EY through the valley due to topographical influences on the local winds. Potential sediment sources for the dune field were identified and investigated by studying thermal inertia and mineralogy. The topographic slope-related katabatic winds travel down the valley walls and converge with the dominant winds travelling through the center of the valley, causing overall eastwards dune migration. Topography is likely the dominant control on the local wind regime; slope winds travel down the sides of the valley walls and are funneled through the center of the valley. These local winds subsequently facilitate the migration of the large dunes in Coprates Chasma, thus expanding our understanding of local winds in the martian environment.

Plain Language Summary

Sand dunes and dune fields are common on Mars. Wind erosion and the formation of dunes and ripples are one of the dominant active surface processes on Mars. Localized winds allow dune movement to occur and measuring how fast the dunes and ripples are moving is important for understanding the martian environment. We can monitor the movement of dunes and ripples by using high resolution (0.25 m/px) and medium resolution (5-6 m/px) satellite images. Measuring the migration of the dunes and ripples in Valles Marineris (the largest canyon in the solar system) allows inferences to be made about present-day wind regime. We found the valley topography and steep slopes may accelerate the winds travelling eastwards through the valley, which converge with winds travelling down the valley slopes. It is likely that these combined winds facilitate the erosion of several source regions, supplying sand to the dune field enabling the migration of the large dunes and ripples. These results highlight the effects of topography on local winds and the influence a wind regime has on large dunes.

1 Introduction

Aeolian erosion and deposition are one of the dominant surface processes on Mars (Bourke *et al.*, 2008; Bridges *et al.*, 2012b; Chojnacki *et al.*, 2019) and probably played important roles throughout the evolution of its surface (e.g. Banham *et al.*, 2018). Sand dunes, which were first observed on Mars by the Mariner 9 (~1 km per pixel) orbiter (Sagan *et al.*, 1972), are still being observed and monitored today in high resolution datasets collected by the Mars Context Camera (CTX; 5-6 m per pixel; Malin *et al.*, 2007) and High Resolution Imaging Science Experiment (HiRISE; 0.25 m per pixel; McEwen *et al.*, 2007) camera on board the Mars Reconnaissance Orbiter. Observing and monitoring sand dunes allows us to learn more about the martian climate and environment, because active aeolian systems are found in numerous, diverse locations across the martian surface (e.g., Banks *et al*., 2018; Chojnacki *et al*., 2019). Comparisons can be made between individual active aeolian systems in different

locations, thus deepening the understanding of dune dynamics and migration rates on Mars as well as wind regimes and atmospheric circulation patterns.

Active sand transport and migration of bedforms within aeolian systems on Mars has previously been investigated using multi-temporal HiRISE (e.g. Silvestro *et al.*, 2010; Bridges *et al.*, 2012b; Cardinale *et al.*, 2016; Runyon *et al.*, 2017; Chojnacki *et al.*, 2019) and CTX images (Davis *et al.*, 2020a). The migration and sediment fluxes of dunes and ripples can be precisely quantified using both manual supra-pixel displacement measurements (Chojnacki *et al.*, 2019) and automated sub-pixel change detection software, such as COSI-Corr ("Co-registration of Optically Senses Images and Correlation"; Leprince et al., 2007) an add-in to the ENVI (ENvironment for Visualising Images) tool suite. COSI-Corr was initially created to measure surface deformation associated with seismic activity and earthquakes (Hollingsworth *et al.*, 2012), but has since been applied to measure dune migration (Vermeesch and Drake, 2008; Necsoiu *et al.*, 2009), terrestrial glaciers (e.g., Herman *et al.*, 2011), landslides (e.g., Le Bivic *et al.*, 2017) and searches for marsquakes (Grindrod *et al.*, 2018).

On Mars, the migration of aeolian bedforms has been measured using both COSI-Corr and manual displacement measurements at numerous dune fields in a variety of different settings, including, but not limited to: Endeavor crater (Chojnacki *et al.*, 2011), Nili Patera (Silvestro *et al.*, 2010; Bridges *et al.*, 2012a; Ayoub *et al.*, 2014), Herschel crater (Runyon *et al.*, 2017), Gale crater (Silvestro *et al.*, 2016), Rabe crater (Fenton, 2006) and as part of planet wide studies (Bridges *et al.*, 2012b; Chojnacki *et al.*, 2019). These studies and others showed that migration rates of dunes and ripples vary across the planet (e.g., Banks et al., 2018; Chojnacki et al., 2019) and within individual dune fields, for example in the particularly high flux region of Nili Patera. At Nili Patera ripple migration reached up to 9 myr^{-1} (Bridges *et al.*, 2012a), whereas the dunes at Herschel crater migrated 0.22 myr^{-1} and ripple displacement was 1.1 m (Cardinale *et al.*, 2016; Runyon *et al.*, 2017). Regardless of location, these studies show that martian bedforms have lower sediment fluxes in comparison to most terrestrial aeolian systems (Vermeesch and Drake, 2008).

Another location where dune fields are common is Valles Marineris, (Chojnacki *et al.*, 2014a,b), Mars' equatorial canyon system. The depth of the Valles Marineris canyon creates unique wind conditions, but the effects of the dramatic topography on aeolian systems in Valles Marineris has not been fully explored. Valles Marineris is a major sediment sink on Mars and contains approximately a third of the non-polar dune fields (Chojnacki and Moersch, 2009; Chojnacki *et al.*, 2014a,b). Chojnacki *et al.* (2014b) compared dune fields in Valles Marineris to other mid to low latitudes (50°N-50°S) dune fields, finding strong differences in composition, morphology and thermophysical properties. The study concluded that the dune fields present in Valles Marineris are quantitatively and qualitatively different to dune fields elsewhere on Mars (Chojnacki *et al.*, 2014b). We argue that the dunes in Coprates Chasma experience both slope winds, created by the large pressure differences between the base of the valley and the top of the ~7 km valley walls, and forced regional winds that are channeled through the valley. The convergence of both these winds may facilitate the movement of large dunes present in the canyon.

In this study, we investigated a 10 km long dune field in Coprates Chasma, one of the southern canyons of Valles Marineris. The Coprates Chasma dune field contains some of the tallest dunes on Mars and a potential sediment source is found upwind of the dunes. We used a combination of HiRISE and CTX images and topographic datasets to investigate the dune field. We used multi-temporal HiRISE images to quantify migration rates and sand fluxes

within the dune field, using a combination of both manual measurements and change detection software (COSI-Corr). We also compared the thermophysical and mineralogical properties of the dunes and potential sediment sources using Thermal Emission Imaging System (THEMIS; Christensen *et al.*, 2004; Fergason *et al.*, 2006) and Compact Reconnaissance Imaging Spectrometer for Mars (CRISM) (Murchie *et al.*, 2007) datasets. Finally, we discuss the influence of complex wind regimes on the dune field and implications for the wider region.

2 Geological Setting

Our study site (Figure 1) is in southern Coprates Chasma, located in the southeast of Valles Marineris. Valles Marineris is a structural extensional rift system and is the largest canyon on Mars (Blasius *et al.*, 1977; Frey, 1979). The whole system is ~3000 km in length, reaches depths of 7 km, and features present include aeolian bedforms (Chojnacki and Moersch, 2009). Valles Marineris is aligned radially to Tharsis and likely formed by a combination of vertical subsidence and modest extension, enhanced by erosion and sedimentation from a variety of sources (Andrews-Hanna, 2012). The depth of the valley creates unique wind conditions whose effects on dune migration rates have not been fully explored before.

Southern Coprates Chasma is 20 km in length and the maximum width of the canyon at the dune field here is 11 km. The canyon walls are steeply sloped (up to 82°, average slopes 30-40°) and reach depths of ~7 km. In the center of the valley, there is a large (~10 km in length and ~11 km width) dune field, which at its maximum extent fills the width of the canyon. The dune field lies on the floor of the valley, which is dipping to the west (Figure S1). The dune field comprises both barchan and barchanoid dunes (Figure 2), which have east and southeast orientated slip faces (i.e., along the canyon axis) and some of the dunes extend up onto the lower canyon walls. The dune field contains dunes with a mean height of ~50 m, with the largest dunes reaching heights of ~180 m, measured from the CTX DTM. Adjacent to the dune field are a series of light-toned alluvial fans and bajadas on both the north and south canyon walls (Grindrod *et al.*, 2019). Previous work has suggested that the lower Coprates wall slopes are the likely sources of sediment for the dune field (Chojnacki *et al.*, 2014a). Approximately 20 km west-northwest of the dune field, layered sediment deposits occur. These comprise, dark partially consolidated materials, which acts as a resistant layer that protects lighter toned deposits beneath. In this paper we discuss the likelihood and implications of the dark partially consolidated sediments as a potential source to the dune field and possible other sources.

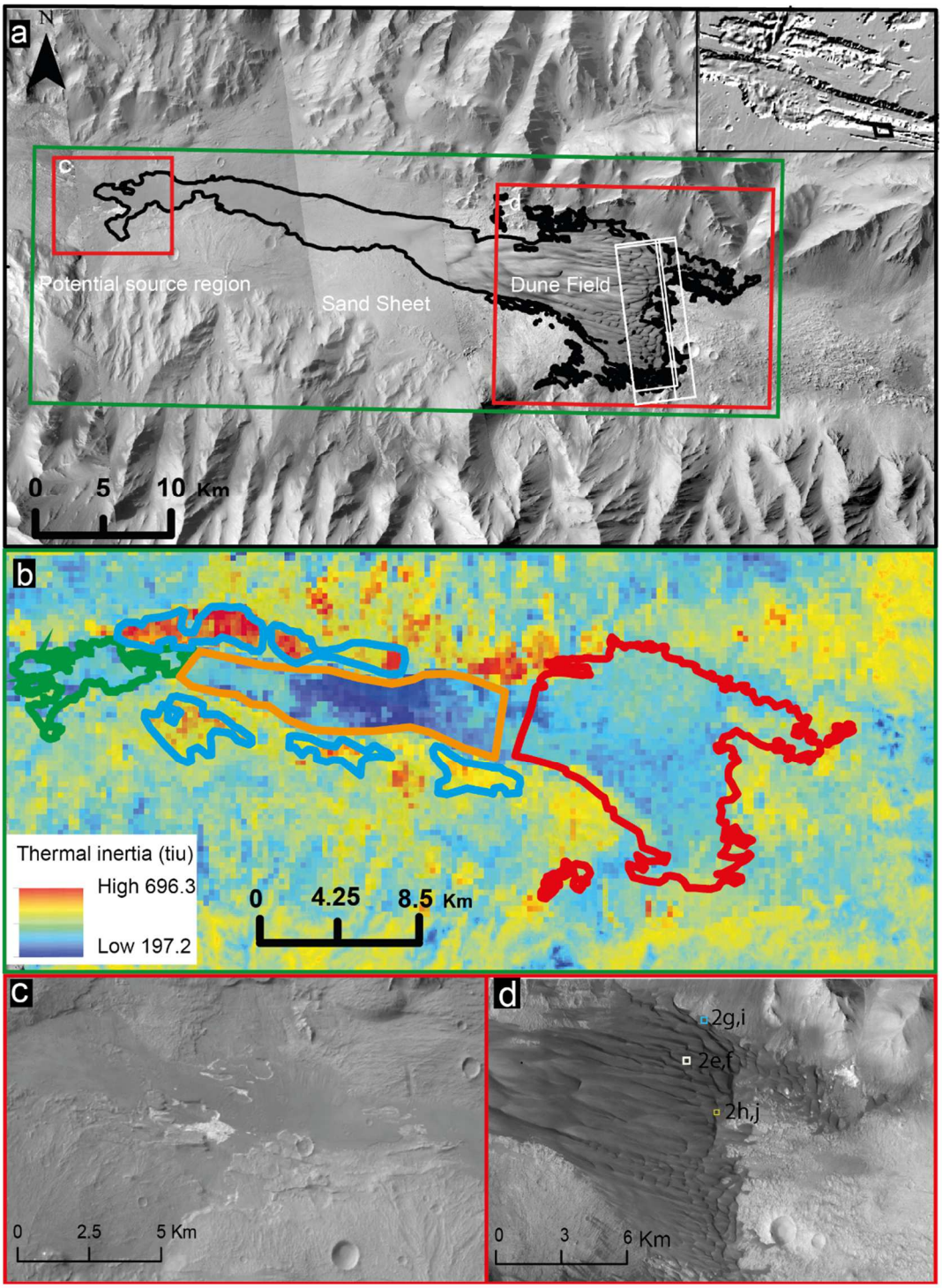

Figure 1. a) Mosaic of CTX images: B18_016844, B19_017200, D21_035331, J01_045129, B22_018123, P08_004067 and D08_030439. The white boxes over the dune field shows the HiRISE footprints showing the dune front and the dunes measured for this study. The red box shows the location of c and d. The context image shows the location of the dune field within Valles Marineris, highlighted by the black box. b) Thermal Emission Imaging System (THEMIS) map overlaid on the CTX image mosaic of the valley. High thermal inertia shown in red and low thermal inertia in blue. The outlined sections show where the thermal inertia measurements were taken for Figure 4: potential source region (green), bajadas (blue), sand sheet (orange) and dune field (red). c) The potential source region located west of the dune

field. d) The dune field within Coprates Chasma. Small white box shows location of e and f in Fig 2, blue box shows location of g and i in Fig 2 and yellow box shows location of h and j in Fig 2.

3 Data and Methods

3.1 Data

We used a combination of images, topography data and thermal datasets to investigate the morphology, morphometry and migration rates of the dune field in Coprates Chasma. We primarily analyzed dune features as well as ripple and dune displacement using HiRISE images (0.25 m/px) and Digital Terrain Models (DTMs; 1 m/px), which were acquired from the NASA Planetary Data System (PDS). Context of the dune field was provided from CTX images (5-6 m/px). The repeat acquisition of both HiRISE and CTX images from 2007 to 2014, provides a time coverage of seven Earth years (EY) for the Coprates Chasma dune field making it an ideal study location. We used THEMIS global thermal inertia maps, which were acquired from the USGS (Christensen *et al.*, 2004; Fergason *et al.*, 2006) to make comparisons of the thermal inertia of the dune field, potential source region, and valley slopes. CRISM images were used to analyze the mineralogical composition of the dunes and potential sources.

3.2 Stereo Digital Terrain Models (DTMs) and Ortho-Rectified images

We used a HiRISE 1 m DTM made with the stereo pair images ESP_031995_1660 and ESP_031929_1660, as well as accompanying ortho-rectified images (Table 1) (0.25 m/px), from the NASA PDS to measure the ripple movement on the stoss slope of the dunes and to measure the dune brink movement. We produced a CTX DTM of the dune field (spatial resolution 20 m/px, vertical precision ~5 m) using the USGS Integrated Software for Imagers and Spectrometers (ISIS) software and the BAE photogrammetric package SOCET SET with CTX images F10_039683_1658 and F11_040039_1660, following the method of Kirk *et al.* (2008).

3.3 Morphometry

We measured the morphometry (height, length, crest length and orientation) of 115 dunes at the front of the Coprates Chasma dune field by digitizing these features using ArcGIS software and a CTX DTM. The dunes analyzed had a visible crest and slip-face. These CTX measurements were used to calculate mean morphometric values of the dunes, which covers a large part of the dune field and assisted mass balance calculations for volume estimation. We also measured the maximum dune height, of 21 dunes at the dune front (used to analyze the ripple and crest movement), by taking profiles across the dunes using the HiRISE DTM and compared both the CTX and HiRISE results where there was dual coverage. We used the HiRISE DTM measurements to calculate the crest flux of the dunes as it has a higher spatial resolution.

3.4 Thermal Inertia

Thermal inertia is defined as $I=(k\rho c)^{1/2}$ where k is thermal conductivity, ρ is bulk density of the material and c is the specific heat capacity representative of the upper few centimeters of the surface. Thermal inertia is partly a function of the composition of the surface material, but other factors, such as grain size, induration etc., are also important. Thermal inertia values were extracted using ArcGIS from the THEMIS global maps (Christensen *et al.*, 2004;

Fergason *et al.*, 2006) for the dune field (Chojnacki *et al.*, 2014a): individual dunes (same dunes as measured for morphometry), the sand sheet on the floor of the valley, the bajadas at the base of the valley walls and the dark partially consolidated sediment at the upwind end of the dune field, which we hypothesize is a potential source region for the dune field. From these values, inferences were made about aeolian transport within the valley.

3.5 CRISM

We used Compact Reconnaissance Imaging Spectrometer for Mars (CRISM; (*Murchie et al.*, 2007)) hyperspectral data from the PDS Geosciences Node to analyze the mineralogical composition of the dunes and potential source regions. We used standard processing and analysis techniques described in detail in previous studies (e.g. *Murchie et al.*, 2009), but outlined here. Despite repeat coverage, we identified only two CRISM images to be suitable for this study (Figure 5). For the source region, we used the Map-projected Targeted Reduced Data Record (MTRDR; (*Seelos et al.*, 2016)) product FRT0000ABB7, for which all pre-processing had already been carried out. For the dune region, we used the Full Resolution Short (FRS) product FRS00028DE9, which required pre-processing with the CRISM Analysis Toolkit (CAT; (*Seelos et al.*, 2011)). For both data sets, spectral parameters, which highlight visible and near-infrared spectral features, were produced (*Pelkey et al.*, 2007; *Viviano□Beck et al.*, 2014) and then flattened, to reduce the effect of the 'spectral smile' (*Murchie et al.*, 2007). Spectra of Regions of Interest (ROIs) were taken of apparent consistent units, typically several hundred pixels in size. Due to difficulty in selecting a spectrally-bland region we follow previous studies (e.g. *Ehlmann et al.*, 2009) in using unratioed CRISM spectra in our analyses, resulting in more instrumental and atmospheric noise in our spectra than would be present in ratioed spectra (e.g. *Bishop et al.*, 2009). Finally, these spectra were compared to laboratory spectra taken from the Reflectance Experiment Laboratory (RELAB) Spectral Library. Given the composition of the ROIs, we also used the modified Gaussian model (MGM) approach (*Sunshine and Pieters*, 1993) to study the relative pyroxene abundances, following previous CRISM studies (e.g. *Flahaut et al.*, 2011; *Parente et al.*, 2011; *Skok et al.*, 2012).

3.6 Ripple Migration

We measured the ripple migration rates using sub-pixel correlation of HiRISE images with the COSI-Corr software package following well-validated methods (Vermeesch and Drake, 2008; Bridges *et al.*, 2012a; Silvestro *et al.*, 2016). We combined HiRISE DTMs with orthoimages in COSI-Corr to measure the displacement of the ripples over multiple time-periods from 2007-2014. We correlated the images using a window size of 512 by 512 and a step size of 16, because given the size of the dunes and the resolution of the HiRISE images, these were the optimum parameters for measuring migration of the ripples, which consistently produced the best output. We calculated the magnitude and direction of the displacement by combining the two component displacement directions following the robust migration direction (vector average) method (Necsoiu et al., 2009; Baird, Bristow and Vermeesch, 2019). Stacked profiles over 21 dunes, found near the front, eastern edge of the dune field (Figure 6), were taken and averaged to calculate ripple displacement. Ripple height was not resolvable in the HiRISE DTM. As the ripples in Coprates Chasma are broadly similar in dimensions to those measured in Nili Patera by Bridges et al. (2012), we assumed a

mean ripple height of 0.2 m. Mis-registration was measured using the same method for measuring the ripple migration, but by measuring any displacement over an area of static bedrock (Figure 6).

3.7 Dune Migration

We manually measured the migration rates of the dunes by mapping the dune brink over a time period of seven years from 2007 to 2014. We mapped the dune brink of the same 21 dunes at the dune front collocated with the ripple displacement measurements. Following previous studies (Chojnacki *et al.*, 2011; Chojnacki, *et al.*, 2019), the dune brink displacement was measured using the migration of the central point of the dune brink relative to the 2007 base image to images of increasing time intervals, for instance 2007 to 2012 or 2007 to 2013. Brink displacements were found to be a more reliable metric to measure because the base of the lee slopes in the HiRISE images were in shadow, hindering their identification. In this study we present only the results for a time gap of 4.7 EY as these images showed the best orthorectification and co-registration. As the dunes are slow moving the displacement is small and therefore the co-registration of the images needs to be precise in order to ensure the displacement measured is not an artifact of co-registration issues. The orthorectification and co-registration in the dune field is complicated by the steep topography and the lack of texture across the dune field as well as changes in light and shadows. For the time period 4.7 EY we observed significant displacement of several meters for several of the dunes (Figure 8, S2), which was greater than any mis-registration between images. The migration rate was calculated using displacement measured divided by the time-period (measured in Earth years, Table 1) over which the displacement had occurred. We calculated an approximate crest flux of the dunes by multiplying the migration rate by the measured HiRISE dune height, as is standard for planetary aeolian studies of barchan dunes (Bridges *et al.*, 2012a; Chojnacki *et al.*, 2019).

Manual dune Migration Measurements				**COSI-Corr Ripple migration Measurements**			
Time Period (EY)	**HiRISE Images**	**Acquisition date (mm/dd/yyyy)**	**Solar Longitude (°)**	**Time Period (EY)**	**HiRISE Images**	**Acquisition Date (mm/dd/yyyy)**	**Solar Longitude (°)**
4.7	PSP_006480_1660 ESP_28804_1660	12/14/2007 09/17/2012	2.3 173.4	0.7	ESP_028804_1660 ESP_031929_1660	09/17/2012 05/19/2013	173.4 321.1
				1.5	ESP_028804_1660 ESP_036320_1660	09/17/2012 04/26/2014	173.4 121.9
				4.7	PSP_006480_1660 ESP_028804_1660	12/14/2007 09/17/2012	2.3 173.4
				5.4	PSP_006480_1660 ESP_031929_1660	12/14/2007 05/19/2013	2.3 321.1
				6.8	PSP_006480_1660 ESP_038430_1660	12/14/2007 10/07/2014	2.3 210.1

Table 1. Images used for ripple and dune migration measurements.

4 Results

4.1 Morphology and Morphometry of the Coprates Chasma Dunes

The Coprates dune field has migrated along the length of the canyon leaving a remnant sand sheet ~16 km long, which contains bright, decameter scale TARs. Some of these bedforms appear indurated as they are crater-retaining. Closer to the dunes, the remnant sand sheet transitions into an active sand sheet ~7 km long, containing dark, meter-scale ripples. Towards the rear of the dune field and sand sheet we observe dunes that have a linear appearance (parallel to canyon length), and which grade into a chain of barchan dunes further to the east (Figure 2c). It is likely that there is a bidirectional wind regime present, indicated upwind by the linear dunes that grade into barchans and the multiple orientations of the ripples on the stoss slopes of the dunes. The Coprates Chasma dune field is dominantly composed of barchan dunes, some of which have coalesced with neighboring dunes to form barchanoid ridge dunes (Figure 2d), most of which have east and southeast orientated slipfaces. This can be seen particularly at the front (east) of the dune field. We also observe climbing dunes on the valley slopes and barchan dunes accumulating on top of each other, where there is a build-up of sediment.

On the stoss slopes of the barchan and barchanoid dunes we observe ripples of varying patterns and orientations. Near the canyon walls, we observe ripples that are orientated in several directions (in some cases, forming a “cross-hatch” pattern; Figure 2g, i), suggesting a convergence of multiple wind regimes. In the center of the dune field we observe ripples, which are orientated perpendicular to the assumed dominant westerly wind direction (along the canyon; Figure 2h, j). We observe dust devil tracks throughout the dune field, which when seen in one HiRISE image, are often not seen in subsequently acquired images, indicating that surface dust is being rapidly cleared (Figure 2a, b). Slope failure, in the form of avalanche-like features, are directly observed at the lee slopes of several barchan and barchanoid dunes, and new activity is seen to occur between HiRISE image acquisitions, indicating that the slipfaces are at or near the angle of repose. Furthermore, slope streaks also appear and disappear in between images, further evidence for avalanching and slope failure along the lee slopes (Figure 2e, f). These observations suggest that the Coprates dunes are

actively migrating. Direct measurements of ripple and dune activity are shown in sections 4.4 and 4.5.

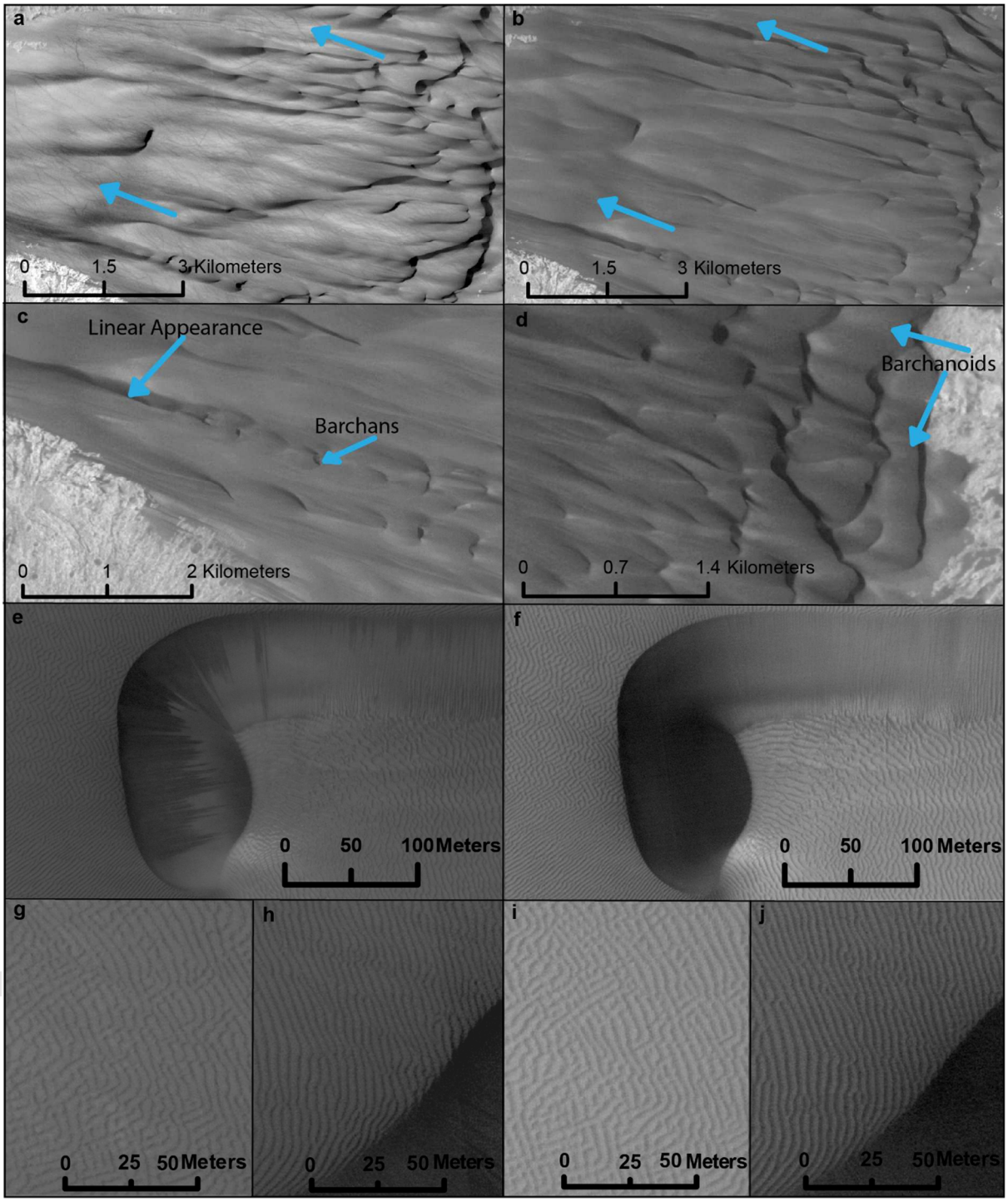

Figure 2. HiRISE and CTX images showing active sediment transport in Coprates Chasma. a) Dust devil tracks seen on the dune field, examples shown by blue arrows, CTX image D19_034698_1658. b) The same area observed ~ 13 months later shows that the dust devil tracks are no longer present, CTX image F10_039683_1658. c) Linear shaped dunes, which then change to barchan dunes, showing a change in the sediment supply, F10_039683_1658. d) Barchanoid dunes seen at the front of the dune field, F10_039683_1658. Location of e to j shown in figure 1d. e) Streaks seen on lee slope, HiRISE image PSP_006480_1660, f) Streaks

no longer seen, HiRISE image ESP_02408_1660. g) Ripples at the north slopes of the dune field, PSP_006480_1660. h) Ripples in the center of the valley, PSP_006480_1660. i) Ripples at the north slopes of the dune field, some change in ripple shape is observed, ESP_02408_1660. j) Ripples at the center of the valley, some change in ripples observed, ESP_02408_1660.

Measuring the dune heights revealed that the barchans and barchanoid dunes at Coprates Chasma are some of the tallest on Mars. CTX measurements showed that the dunes ranged in height from 3 to 182 m. The dunes increase in height towards the north and center of the dune field (Figure 3a). In some cases, there is a good agreement between the height measurements extracted from the HiRISE and CTX DTMs over the same dune (Figure 3d), but for others there are discrepancies between the datasets of up to 57 m (see Davis et al., 2020a for detailed discussion of the possible reasons for this). As such, we only used the height values extracted from the HiRISE DTM for computing the crest fluxes, arguing that this provides more accurate data due to the higher DTM resolution and vertical precision. We found no strong correlation between dune length and dune height nor between dune crest length and dune height, where we would expect dune height to increase proportionally to both dune length and crest length (Figure. 3c and 3d). However, due to the variety in shapes of the dunes, dune crest length and dune length varied widely between the different dunes types observed. Dune crest length ranged from 98-2159 m and dune length ranged from 80-2135 m. The measured orientation of the dune slip faces are east to south-east, with a range in orientation of 57-168°. From the orientation of the dunes, we infer that the dominant dune forming winds are of a westerly direction.

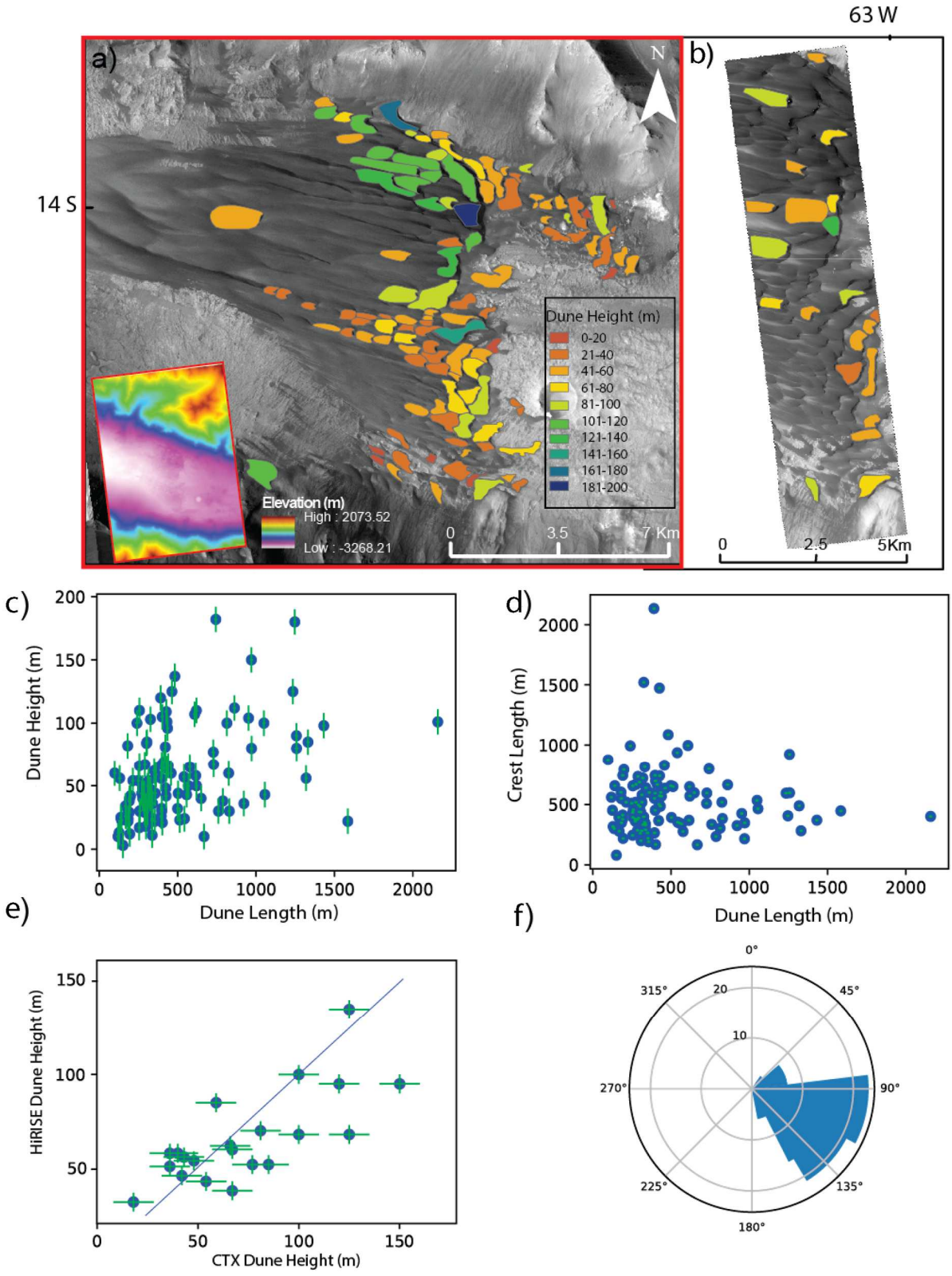

Figure 3. Dune morphometric measurements. a) The CTX derived heights of the dunes showing their location in the dune field. CTX DTM shown in bottom left of image. b) HiRISE derived heights of dunes, which are used to calculate the crest fluxes. c) Scatter graph of the dune length and the dune height. Error bars show the approximated error in the CTX measurements (10 m) from the CTX DTM. d) Scatter graph of the crest length and dune length. Error bars

show the approximated error in the CTX measurements, (10 m) from the CTX DTM. e) Correlation of the CTX height measurements and the HiRISE heights. Error bars show the approximated error in both the CTX and HiRISE height measurements of 10 m and 5 m respectively from both the CTX and HiRISE DTMs. A 1:1 reference line is drawn. f) Rose plot showing the orientation of the dunes. The radial axis is the number of dunes and the direction axis indicates the facing direction of the slipface.

4.2 Thermophysical Properties of the Study Area

Thermal inertia was measured from global THEMIS TI (thermal inertia) datasets. Figure 4 shows the variation between the TI values of the dune field and the valley floor. There are large differences, of the order of 200 Thermal Inertia Units (tiu, = J m^{-2} K^{-1} $s^{-½}$), in the TI of the bajadas on the floor of the valley, the sand sheet and the dark areas in the west that are the potential sand source region. The TI of the bajadas range from 500-600 tiu and the sand sheet and the potential source region have a lower TI of 300 and 200-250 tiu respectively. There is a variation in the thermal inertia values of individual dunes, from 312-490 tiu, with a mean of 378 tiu. The individual dune values for thermal inertia are more similar to those of the potential source region than those of the bajadas.

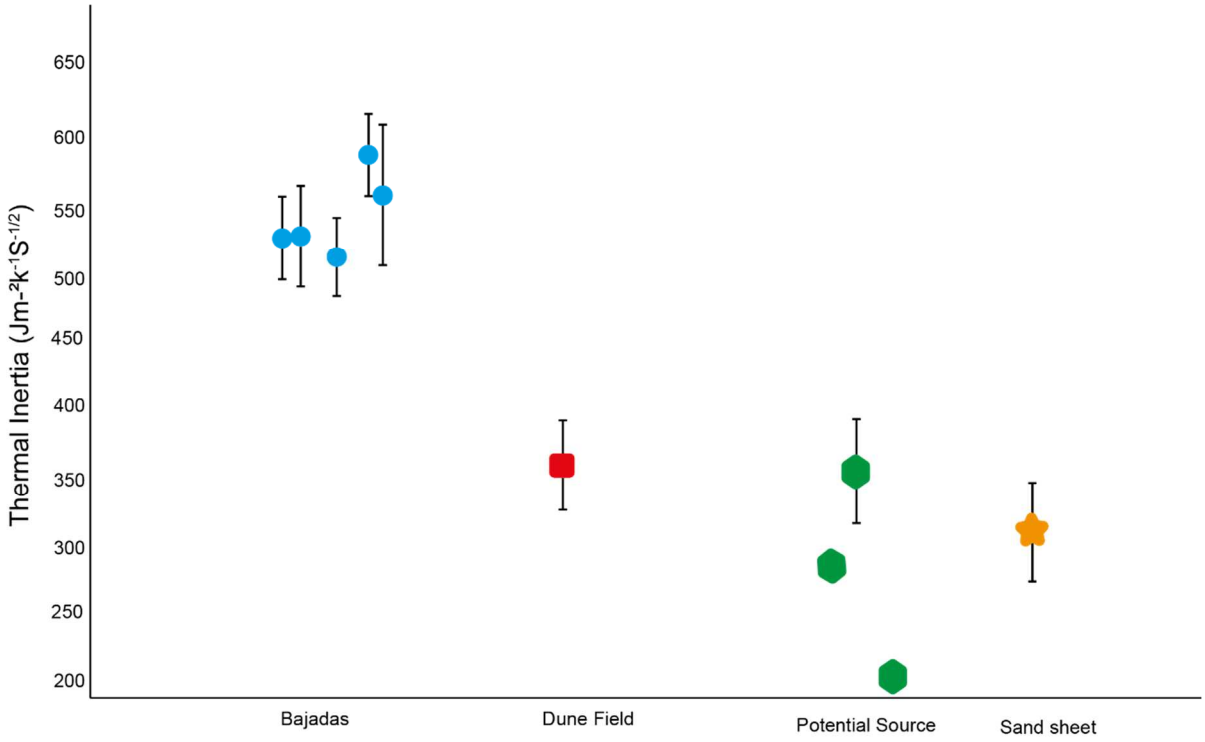

Figure 4. Thermal inertia plot showing mean values and the standard deviation for different features within the valley.

4.3 Mineralogical Analysis

We used our CRISM analyses to compare the mineralogical composition of the dunes and possible source region (Figure 5). In the potential source region, the dark mantling unit has an overall composition that differs from the surrounding alluvial fans and bajadas. The source region ROI spectrum, although suffering from noise, is most typical of pyroxene, and the broad absorption feature at 2.3 μm is indicative of HCP. The normalised low calcium pyroxene band

depth' (NBDLCP) spectral parameter map shows that this HCP composition tends to dominate the dark mantling unit, although with some smaller areas that could be richer in LCP, which tend to be at the erosional edges of alluvial fans and bajadas. In the dune front area, although the CRISM data are noisier than in the source region, it is still evident that the dunes have an overall composition that is distinct from the surrounding canyon floor material. The dune ROI spectrum has a broad absorption feature at 2.2 μm that is again indicative of HCP, although with a possible small increase in LCP contribution. The NBDLCP spectral parameter map shows that this HCP composition generally is strongest in the dunes. Conversely, most areas that are richer in LCP tend to occur in the canyon floor material, although there are small areas within the dunes that could contain more LCP. In summary, although not definitive, the composition of the possible source region has mineralogical similarities to that of the dunes, but there remain some apparent differences that could be due to other source regions.

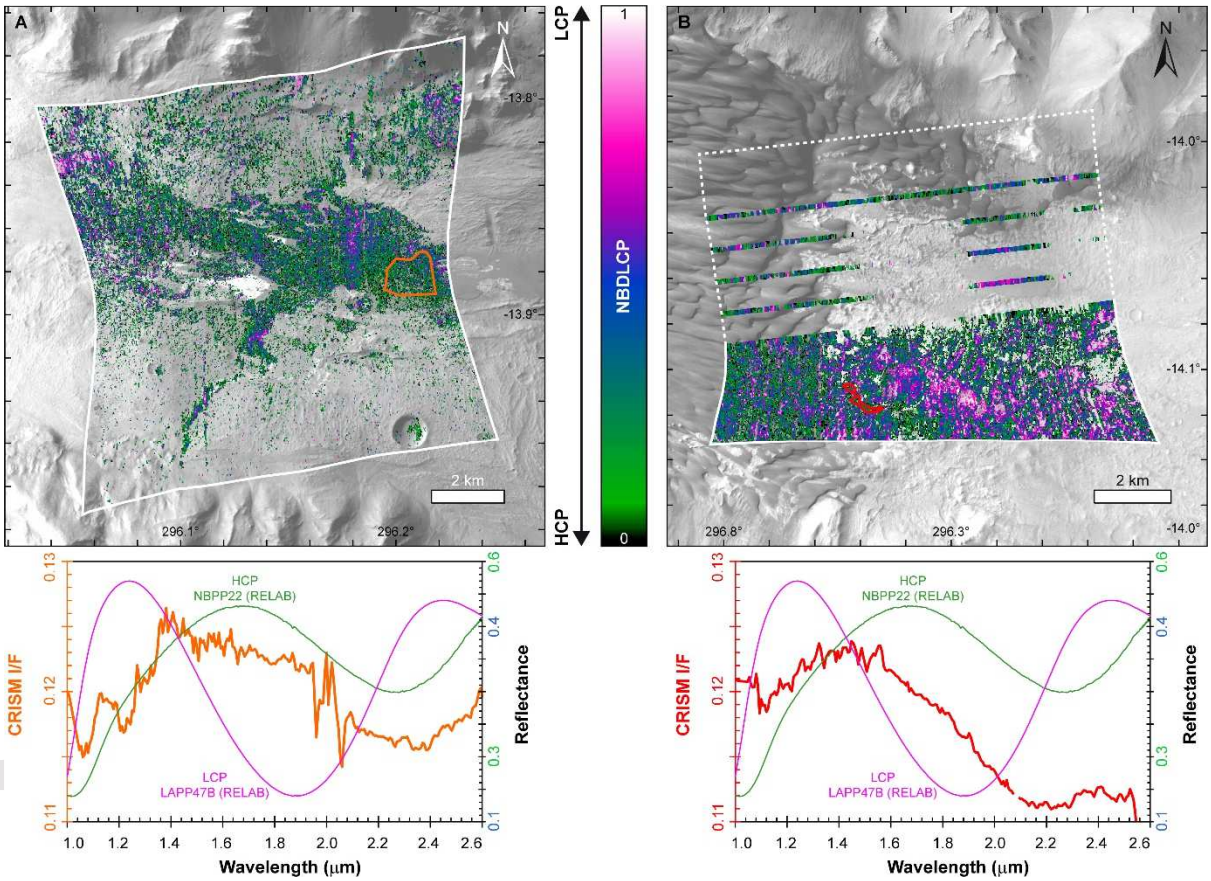

Figure 5. CRISM analysis of (A) potential source region and (B) study dunes. In each case the top image shows the MGM-produced spectral parameter 'normalised low calcium pyroxene band depth' (NBDLCP), representing the relative abundance of low calcium pyroxene (LCP) and high calcium pyroxene (HCP), overlain on a CTX base image. Colored polygons represent regions of interest (ROIs) for spectra. Below in each case are ROI-derived CRISM spectra (left axis) and RELAB spectral library spectra for LCP and HCP.

4.4 Ripple Migration and Sand Fluxes

COSI-Corr was successfully used to measure the migration of the ripples on the stoss slopes of the 21 dunes using multi-temporal HiRISE data across all five time periods (Figure 6). The ripple displacement varied across the 21 dunes from 0.4 to 18.3 m with overall geometric mean displacement for the maximum time-period (6.8 Earth years) of 5.98 ± 4.5 m. As

expected, ripple displacements increased with time, with mean displacements of 2.6 m, 3.7 m and 5.1 m for 1.5 year, 4.7 year, and 5.4 year time gaps respectively (Figure 7). The COSI-Corr data had a high signal to noise ratio (SNR) for the 1.5 and 0.7 year time gaps, however there was a lower signal to noise for data over longer time gaps (Figure 6), which could suggest there are some aliasing issues over the longer time gaps. The displacement values give mean annualized migration rates of 0.8-1.2 m/EY across all time intervals. Assuming a ripple crest height of 0.2 m (Bridges *et al.*, 2012b; Lapotre *et al.*, 2016), the ripples therefore have a mean crest flux of 0.4-0.6 m^3 m^2 EY^{-1} across all time intervals. We observed lower displacement rates and therefore lower ripple fluxes over longer time periods, typical of nonstationary phenomena (Mandelbrot and Wallis, 1968; Sadler, 1981). To ensure images were sufficiently well orthorectified, the displacement over bedrock in each correlation was measured. The mis-registration error for all time periods (0.4 ± 0.03, 0.3 ± 0.03, 0.3 ± 0.06, 0.6 ± 0.07, 0.5 ± 0.06 m) was low, and less than the ripple displacement in all cases (Figure 7). Our results (Table 2) suggest that ripple migration rates are around 1 m/EY, and the geometric mean ripple flux was 0.5 m^2/EY, assuming 0.2 m ripple height.

Table 2: Average Ripple Displacement Rates Across the Dune Field.

Time period (EY)	**Displacement rate (myr^{-1})**	**Ripple Flux ($m^3m^{-1}yr^{-1}$)**
0.7	1.0 ± 1.3	0.5 ± 1.3
1.5	1.2 ± 1.3	0.6 ± 1.3
4.7	0.8 ± 1.4	0.4 ± 1.4
5.4	0.8 ± 1.5	0.4 ± 1.5
6.8	0.8 ± 1.5	0.4 ± 1.5

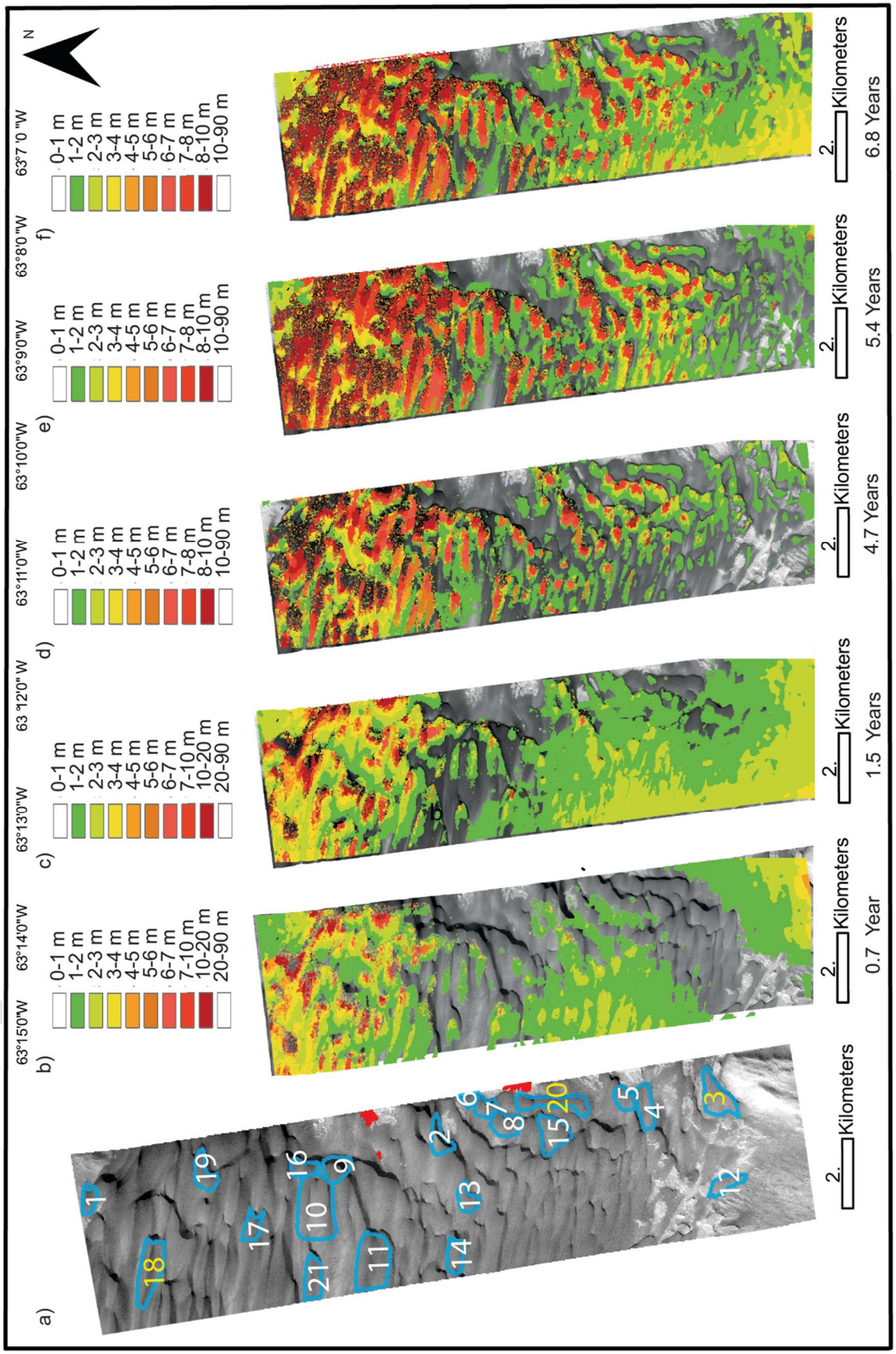

Figure 6. Displacement of the ripples on the stoss slopes of dunes for several time-periods. Green-yellow shows areas with less displacement and red shows areas of higher

displacement. (a) HiRISE image showing the 21 dunes used to measure ripple migration by COSI-Corr outlined in blue and labelled in white. The dunes labelled in yellow were also used for manual measurements. Red polygons show the locations of where bedrock was measured to calculate the mis-registration error for each of the COSI-Corr correlations. (b) Ripple displacement over 0.7 EY (2013-2014). (c) Ripple displacement over 1.5 year (2012-2014). (d) Ripple displacement over 4.7 EY (2007-2012). (e) Correlation start to appear more pixelated towards northern slopes, possibly due to aliasing issues. Ripple displacement over 5.4 EY (2007-2014). (f) Ripple displacement over 6.8 EY (2007-2014) Correlation appear more pixelated towards northern slopes, possibly due to aliasing issues. Note that the ripple displacement increases with time and for all correlations a filter of SNR > 0.9 was applied to all results.

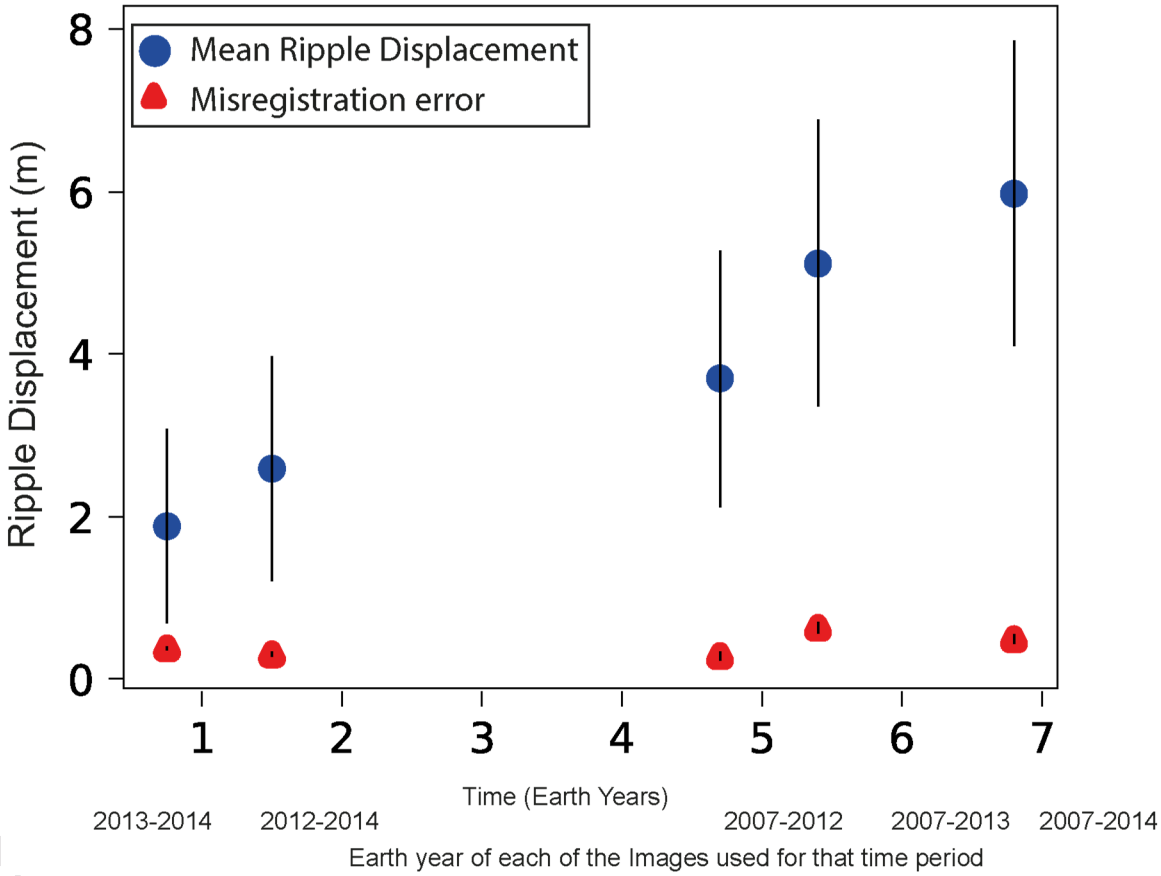

Figure 7. Geometric mean displacement of the ripples over time. Error bars are standard error of the geometric mean. Mis-registration error shown as red triangles

4.5 Dune Migration and Sand Fluxes

We measured the displacement of the dune crests over multiple time periods. In many cases, we found that poor image co-registration meant that the displacement values could not be accurately measured (i.e., there was significant mis-registration over static bedrock areas). However, good image co-registration between HiRISE images PSP_006480_1660 and-ESP_28804_1660 allowed us to accurately measure the displacement of several dunes over 4.7 EY. Some dunes displayed large displacements over this time period with displacements greater than 1 m in some cases. Dune displacement varied between 0.6-1.3 m giving a displacement rate between 0.1-0.3 m/EY (Table 3, Figure 8). Displacement uncertainty was assumed to be 2 HiRISE pixels (0.5 m), which we estimate as the likely error when measuring the distance between the identified 2D crest line of the dunes in each image. The

dunes are migrating at different rates across the dune field, due to their location within the dune field and the height of the dunes, but the dune field is actively migrating generally eastwards. The dunes that showed the largest displacements are all less than 100 m in height and are some of the smaller dunes in the dune field. Displacement is proportional to height, with smaller dunes moving faster. The larger dunes in the dune field are probably still active, but are moving at a rate that cannot be reliably measured over the time period the images were taken.

Table 3. Dune Displacement Rates and Crest Fluxes.

Dune Number	**Height (m)**	**Time Period (Earth Years)**	**Displacement (m)**	**Displacement rate (myr^{-1})**	**Crest Flux ($m^3m^{-1}yr^{-1}$)**
3	68 ± 5	4.7	0.64 ± 0.5	0.14 ± 0.11	9.48 ± 7.44
18	68 ± 5	4.7	0.62 ± 0.5	0.13 ± 0.10	9.17 ± 7.43
20	95 ± 5	4.7	1.27 ± 0.5	0.28 ± 0.11	26.23 ± 10.42

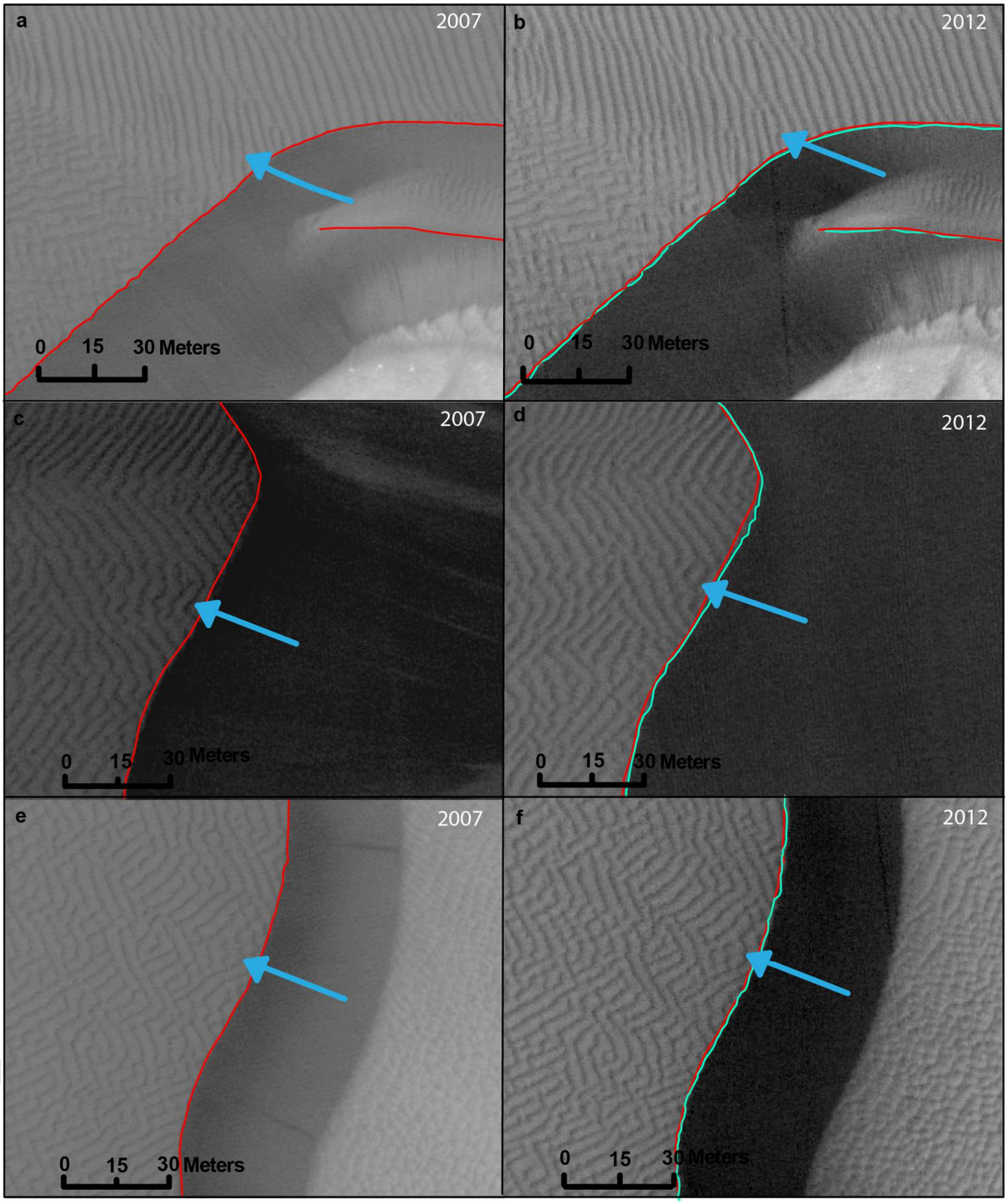

Figure 8. Examples of dune brink displacement for the 4.7 year time period, arrows show an example of ripple changes. Red outline shows the outline of the dune brink from HiRISE image PSP_006480_1660 (2007), turquoise line shows the outline of the dune brink in image ESP_028804_1660 a) Dune 3, PSP_006480_1660, b) Dune 3 ESP_028804_1660, c) Dune

18, PSP_006480_1660, d) Dune 18, ESP_028804_1660, e) Dune 20, PSP_006480_1660, f) Dune 20, ESP_028804_1660.

5. Discussion

5.1 Inferring Potential Sediment Sources for the Dunes

In this study we have investigated the possible sources of the dune field and consider one such potential source region westward of the dune field. If this region alone is sourcing the dunes, then the dune field could be considered to effectively have a point source (Ewing and Kocurek, 2010). The Coprates Chasma dune field is composed of a large volume of sand shown by the height of the dunes, it is particularly noteworthy that these dunes are migrating, suggesting an efficient and possibly complex wind regime is present within the valley. The variation in crest length and dune lengths, with linear dunes that evolve into a chain of barchans towards the rear of the dune field is observed elsewhere on Mars in relatively sediment starved regions; Davis *et al.*, 2020b. Linear dunes are observed in our study region, and require a bidirectional wind regime (e.g. Tsoar, 1989; Gao *et al.*, 2015), which in this case could be due to katabatic winds travelling down the canyon slopes combining with winds travelling eastwards through the valley. Barchan dunes form when there is low sediment supply (Bourke and Goudie, 2009; Gao *et al.*, 2015; Runyon *et al.*, 2017), but in the center of the valley these barchans coalesce with neighboring barchans forming barchanoid ridges, possibly reflecting a higher sediment supply. Therefore we do not observe the same patterns in dune distribution expected from a point source, as suggested by Ewing and Kocurek in their 2010 study.

Alternatively there could be multiple point and plane sources to the dune field, possibly including the identified potential source region, as well as material eroded from the slopes, bajadas at the edges of the valley floor or material from outside of the valley. One consideration is the volume of material needed to source the dunes. The potential source region covers an area of 17 km^2 and the maximum depth is 40 ± 10 m (uncertainty in DTM measurements ~ 2 pixels). Therefore the approximate volume of material that could be eroded from the source region is 0.68 ± 0.17 km^3. The dune field has area of 108 km^2 and mean height of the dunes is 58 ± 10 m (uncertainty in DTM measurements ~ 2 pixels). Therefore the approximate volume of the dune field is 6.25 ± 1 km^3, an order of magnitude greater than the volume of material that could be sourced from the potential source region. This contrast in volume supports the idea of multiple sources to the dunes. If including material eroded from the sediment transport pathway, which has an area of 45.7 km and a depth of 8 m then there is an extra contribution of 0.37 ± 0.37 km^3 giving a total volume from the potential source region and sand transport pathway of 1.05 km^3. The total area of the bajadas measured for thermal inertia is 38 km^2 and the depth varies from 2-10 m giving a maximum volume of material that could be eroded from the bajadas of 0.26 ± 0.2 km^{-3}. The volume of material from the bajadas combined with the volume of material eroded from the sediment transport pathway and the source region is 1.31 km^3, further supporting the idea of multiple sources.

However, our thermal inertia and mineralogy results do support the potential source region being one source to the dunes (Figure 4). The southern Coprates Chasma dunes have low thermal inertia values, which closely match the potential source region and, to a lesser extent, the sand sheet. The differences in the thermal inertia values can be accounted for by whether the material is consolidated or unconsolidated (sand particles), which has a direct impact on the thermal inertia values (Christensen *et al.*, 2004). The material at the potential source

region is comprised of dark-toned, partially consolidated mantling material, and brighter underlying phyllosilicate bearing units. The bajadas and fans show layers of darker material and lighter toned material, and there is evidence of erosion at the edges of the fans of the darker layers (e.g., steep scarps). It is possible that the dark material could be reworked into the potential source region or could be directly sourcing the dunes, suggesting aeolian fractionation could be occurring within the valley. However, the bajadas have distinctively higher thermal inertia values (Figure 4) than the dune field, the potential source region and the sand sheet. This is consistent with previous studies, which showed that the material sourcing the dunes often had higher thermal inertia than the dune field (Chojnacki *et al.*, 2014), explained by preferential erosion and aeolian fractionation. In comparison the material composing the inactive sand sheet is partly consolidated sand (indicated by indurated bedforms, S1), whereas the material in the active dune field is unconsolidated sand particles.

Within the dune field itself, there are some variations in the thermal inertia, the TI of individual dunes fluctuates from 300-500 tiu, consistent with previous studies (Chojnacki. *et al.*, 2014a). These differences could be explained by influx of dust, or sand transport along the valley and into the dune field. Valles Marineris has high dust levels, caused by erosion of the slopes and valley floor by strong winds in the valley (Spiga and Forget, 2009). The presence of dark, loose sediment on the slopes on the Coprates wall slopes also indicates that some sediment input may have also come from the lower canyon walls and these findings are consistent with the inferences of previous studies (Chojnacki *et al.*, 2014a).

CRISM results further support the potential source region sourcing the dunes as both the potential source region and the dune field consist predominantly of HCP, although with some variations in LCP abundances. The variations in composition could be due to additional source region contributions which would introduce different mineralogies.

In summary, the thermal inertia and CRISM values support the hypothesis that one of the sources of sand to the dune field comes from the area we have identified morphologically as a potential source region. However, the potential source region is not a large enough area to source volume of material that creates the dune field, therefore we expect additional material to be sourced from the bajadas along the valley walls (Chojnacki *et al.*, 2014a) and from erosion of the slopes (Spiga and Forget., 2009). There could also be some influx from the plateaus above Coprates Chasma and the surrounding plains, however, no source region and sediment transport pathway for this is apparent.

5.2 Interpreting the Activity of the Dune Field

The Coprates Chasma dune field shows several lines of evidence for active aeolian processes including (1) the crisp dune slip faces (Banks *et al.*, 2018); (2) observed avalanching and slope streaks on slip faces (Figure 2); and (3) dust clearance in between HiRISE images (Figure 2), (4) and clear ripple migration on the dune surfaces (Movie S1 and S2), with increasing displacement for each time step (Figure 7). The measured ripple migration (0.8-1.2 m/EY) was significantly larger than the measured dune migration (0.1-0.3 m/EY), consistent with bedform scaling relationships. Our ripple migration rates were higher than previously measured rates in other locations including Herschel Crater (Cardinale *et al.*, 2016) and Gale Crater (Silvestro *et al.*, 2016), but are similar to some of the higher migration rates identified in a planet wide migration study (Bridges *et al.*, 2012a). Thus, our measured ripple migration rates suggest Coprates Chasma is a high sand flux region.

The patterns of ripple migration are consistent with a bidirectional wind regime. The ripples on the stoss slopes of the dunes show multiple orientations, particularly the dunes that are towards the northern canyon wall slopes where the ripple crest lines form a cross hatched pattern indicative of multiple wind directions (Figure 2g, j). Here, the transverse ripples are forming perpendicular to the wind regime present, indicating that in this region there is a convergence of the slope winds and the westerly winds. This pattern is most clearly seen on Dune 1 located next to the steep slopes (Figure 6), which showed elevated values for ripple migration consistently throughout all time periods, and is likely to be a high sand flux area. In addition, individual dunes with higher ripple displacement also showed greater dune displacement. Similarly, the large displacements measured from the dunes highlighted in Table 3 may also be explained by their location in the dune field. Both Dune 3 and 18 are located close to the south and north slopes of the valley respectively; thus, both the high rates of dune and ripple migration could be explained by the katabatic and anabatic slope winds converging with the westerly winds along the axis of the valley. Dune 20, located at the front of the dune field shows elevated migration rates for both dune and ripple migration, due to its center location at the front of the dune field and therefore is likely to be influenced by the dominant easterly wind direction, rather than the slope winds that dune 3 and 18 experience.

The mean migration rate of the measured dune crests (Dunes 3, 18, 20) over the 4.7 year period was 0.1-0.3 myr^{-1} and the crest flux varied 9.2-26.2 m ^{3}m^{-1}EY^{-1}, these rates of movement are low but the dune sand fluxes are comparable to rates measured in other moderate (> 5 m^{3}m^{-1}yr^{-1}) to high (> 9 m^{3}m^{-1}yr^{-}1) sand flux areas on Mars (e.g. Bridges *et al.*, 2012; Chojnacki *et al.*, 2019). However, the lower migration rates can be explained by bedform scaling relationships, because the dunes present within the Coprates dune field are significantly taller (heights up to ~180 m) than many other active systems measured in previous studies (e.g. Bridges *et al.*, 2012; Chojnacki *et al.*, 2019). Overall, our dune migration measurements in this study may represent particularly high sand flux regions within the dune field. Further evidence still is the dunes are located not on a flat surface. The valley floor that the dunes are situated on dips to the west (Figure S1), indicating that the dunes are not only migrating through the valley, but are climbing the valley floor as well. The combined evidence for active ripples (all over the dune field) and other aeolian changes (e.g. slope streaks, dust clearance) suggest that the wider dune field is active, but is migrating at a rate that is below the detection threshold (i.e., 2 pixels). The movement of such large dunes suggests that there are topographical influences on a localized wind regime present in Coprates Chasma, mobilizing significant volumes of sand. One possible reason for the large size of the Coprates dunes is that the steep valley gradient is acting as a counter to the winds, resulting in the accumulation of large volumes of sand.

A limitation of the ripple migration results is that for the longer time periods there may be some aliasing issues, as demonstrated by the correlations appearing noisier in dunes closest to the northern slopes, (1, 17, 18 and 19; Figure 6).This effect could potentially cause artificially higher ripple migration rates. However, dunes measured in these areas also had similar high migration rates during shorter time periods, where aliasing is expected to be less of an issue. We also avoided measuring areas with a SNR < 0.9, which coincided with dunes with noisy correlation results and possible aliasing effects. We conclude that the higher sand flux regions that we measured towards the north and southern slopes appear to be real, and not an artefact of aliasing.

5.3 Katabatic Winds, Slope Winds and Mesoscale Climate Models

Previous studies using mesoscale climate models have shown that there are katabatic and adiabatic slope winds in Valles Marineris that at night can reach up to 30-40 ms^{-1} (Spiga and Forget, 2009). The steep slopes present in Valles Marineris accelerate the winds (slope winds increase in intensity with steepness of the slopes) and slope winds also tend to increase in intensity when travelling over distances greater than 2 km (Richardson et al., 2007; Spiga, 2010). At Coprates Chasma, the walls of the valley reach up to ~7 km from the valley floor, allowing cold, dry dense air to flow downslope. These slope winds would occur perpendicular to the main wind direction (eastwards, along valley), which causes a convergence of winds, (i.e., a bi-directional wind regime), evidence of which is seen in the cross-hatch ripple patterns on the stoss slopes of dunes closest to the valley walls (Figure 2). The combined influence of the katabatic and slope winds, and the channeled valley winds (Spiga and Forget, 2009), could facilitate erosion to occur of the potential source region, bajadas and the canyon wall slopes, supplying sand to the dune field. Additionally these winds could also transport material from the plateaus above Coprates Chasma. The influence of a bi-directional wind regime is also reflected in the morphology of the dunes.

6. Conclusions

We have investigated the morphology, bedform activity, and source region of the Coprates Chasma dune field. We have demonstrated the dune field is active with dunes brinks migrating at 0.1-0.3 m/EY (crest fluxes: 9.6-26.2 $m^3m^{-1}EY^{-1}$) and a ripple migration rate of 0.8-1.2 m/EY (crest fluxes: 0.4-0.6 $m^3m^{-1}EY^{-1}$). These migration values and crest fluxes are similar to previous dune migration studies on Mars, but the dunes in Coprates Chasma are up to 182 m in height and therefore this dune field has higher sand fluxes than seen previously. We suggest that the channeling of the winds through the valley has eroded the bedrock at the valley floor, including dark, mantling material, west of the dune field and the bajadas at the edges of the valley. We suggest that some of this dark mantle material supplies sediment to a sand sheet and ultimately to the Coprates Chasma dune field. The observed variations in morphology of the dunes and ripple patterns are consistent with a bi-directional wind regime and changing zones of sediment supply across the dune field. We suggest that the steep local topography creates high speed katabatic and anabatic slope winds, which in turn converge with the dominant dune forming westerly winds, to form a bi-directional high speed wind regime. These combined winds are channeled through the valley and subsequently facilitate the migration of the large dunes. Thus, our results highlight the importance of using dune field morphology to understand local wind regimes and environments. Future work should investigate the activity of the Coprates Chasma dunes over longer time periods, when there is sufficient image availability, and further explore the multiple sources to the dune field.

Acknowledgments

SJB is supported by a Science and Technology Facilities Council PhD studentship (ST/R000727/1). PMG and JMD gratefully acknowledge UK Space Agency funding (ST/R002355/1). MRB acknowledges UK SA funding (ST/R001383/1 and ST/R001413/1). TB is supported by a Natural Environment Research Council PhD Studentship (NE/L002485/1). We thank the various Mars instrument teams for their consistent and dedicated work, in particular the HiRISE team for the production of the DTMs and ortho-rectified images. The data products used in this study are available from the HiRISE PDS Node (https://hirise-pds.lpl.arizona.edu/PDS/). The CTX DTM and ortho-rectified images,

shapefiles and data tables are available from figshare (*Boazman, S., J. Davis, and P. Grindrod (2020) CTX DEM and Shapefiles: Coprates Chasma Dunes. figshare. Collection. https://doi.org/10.6084/m9.figshare.c.5198183.v2*).).

References

Andrews-Hanna, J. C. (2012), 'The formation of Valles Marineris: 3. Trough formation through super-isostasy, stress, sedimentation, and subsidence', Journal of Geophysical Research E: Planets, 117(6), 1–20. https.//doi:10.1029/2012JE004059.

Ayoub, F., Avouac, J-P., Newman, C. E., Richardson, M. I., Lucas, A., Leprince, S., and Bridges, N. T. (2014), 'Threshold for sand mobility on Mars calibrated from seasonal variations of sand flux', Nature Communications. https.//doi:10.1038/ncomms6096.

Baird, T., Bristow, C. S., and Vermeesch, P. (2019), 'Measuring sand dune migration rates with COSI-Corr and landsat: Opportunities and challenges', Remote Sensing, 11(20). https.//doi: 10.3390/rs11202423.

Banham, S. G., Gupta, S., Rubin, D. M., Watkins, J. A., Sumner, D. Y., Edgett, K. S., Grotzinger, J.P. et al. (2018), 'Ancient Martian aeolian processes and palaeomorphology reconstructed from the Stimson formation on the lower slope of Aeolis Mons, Gale crater, Mars', Sedimentology, 65(4), 993–1042. https.//doi:10.1111/sed.12469.

Banks, M. E., Fenton, L. K., Bridges, N. T., Geissler, P. E., Chojnacki, M., Runyon, K. D., Silvestro, S. et al. (2018), 'Patterns in Mobility and Modification of Middle- and High-Latitude Southern Hemisphere Dunes on Mars', Journal of Geophysical Research: Planets, 123(12), 3205–3219. https.//doi:10.1029/2018JE005747.

Le Bivic, R., Allemand, P., Quiquerez, A., and Delacourt, C. (2017), 'Potential and limitation of SPOT-5 ortho-image correlation to investigate the cinematics of landslides: The example of "Mare à Poule d'Eau" (Réunion, France)', Remote Sensing, 9(2), 1–15. https.//doi:10.3390/rs9020106.

Blasius, K. R., Cutts, J.A., Guest, J. E., and Masursky, H. (1977), 'Geology of the Valles Marineris: First analysis of imaging from the Viking 1 Orbiter Primary Mission', Journal of Geophysical Research, 82(28), 4067–4091. https.//doi:10.1029/js082i028p04067.

Boazman, S., Davis, J., Grindrod, P. (2020): CTX DEM and Shapefiles - Coprates Chasma Dunes. figshare. Collection. https://doi.org/10.6084/m9.figshare.c.5198183.v2.

Bourke, M. C., Ewing, R., Finnegan, D., and McGowan, H. A. (2008), Migration Rates of Niveo-Aeolian Dunes in Antartica: Implications for Martian Dunes', Paper presented at 39th Lunar and Planetary Science Conference, Contribution No. 1391, p.2166. Texas, United States.

Bourke, M. C., and Goudie, A. S. (2009), 'Varieties of barchan form in the Namib Desert and on Mars', Aeolian Research. https.//doi:10.1016/j.aeolia.2009.05.002.

Bridges, N. T., Ayoub, F., Avouac, J-P., Leprince, S., Lucas, A., and Mattson, S. (2012a), 'Earth-like sand fluxes on Mars', Nature. 485 (7398), 339-42. https.//doi:10.1038/nature11022.

Bridges, N T., Bourke, M. C., Geissler, P. E., Banks, M. E., Colon, C., Diniega, S., Golombek, M.P., et al. (2012b), 'Planet-wide sand motion on mars', Geology. 40(1), 31-34. https.//doi:10.1130/G32373.1.

Cardinale, M., Silvestro, S., Vaz, D. A., Michaels, T., Bourke, M. C., Komatsu, G., and Marinangeli, L. (2016), 'Present-day aeolian activity in Herschel Crater, Mars', Icarus. Elsevier Inc., 265, 139–148. https.//doi:10.1016/j.icarus.2015.10.022.

Chojnacki, M., Banks, M. E., Fenton, L. K., and Urso, A. C. (2019), 'Boundary condition controls on the high-sand-flux regions of Mars', 47(5), 1–4. https.//doi:10.1130/G45793.1/4657361/g45793.

Chojnacki, M., Burr, D. M., Moersch, J. E., and Michaels, T. I. (2011), 'Orbital observations of contemporary dune activity in Endeavor crater, Meridiani Planum, Mars', Journal of Geophysical Research E: Planets, 116(4), 1–20. https.//doi:10.1029/2010JE003675.

Chojnacki, M., Burr, D. M., Moersch, J. E., and Wray, J. J. (2014a), 'Valles Marineris dune sediment provenance and pathways', Icarus. https.//doi:10.1016/j.icarus.2014.01.011.

Chojnacki, M., Burr, D. M., and Moersch, J. E. (2014b), 'Valles Marineris dune fields as compared with other martian populations: Diversity of dune compositions, morphologies, and thermophysical properties', Icarus. https.//doi:10.1016/j.icarus.2013.08.018.

Chojnacki, M., and Moersch, J. E. (2009), 'Valles Marineris Dune Fields: Thermophysical Properties, Morphology and Provenance', Paper presented at 40th Lunar and Planetary Science Conference, Texas, United States.

Christensen, P. R., Jakosky, B. M., Kieffer, H. H., Malin, M. C., McSween, H.Y., Nealson, K., Mehall, G.L., et al. (2004), 'The Thermal Emission Imaging System (THEMIS) for the Mars 2001 Odyssey Mission', Space Science Reviews. https.//doi:10.1023/B:SPAC.0000021008.16305.94.

Davis, J. M., Banham, S. G., Grindrod, P. M., Boazman, S. J., Balme, M. R., and Bristow, C. S. (2020b), 'Morphology, Development, and Sediment Dynamics of Elongating Linear Dunes on Mars', Geophysical Research Letters, 0–3. https.//doi:10.1029/2020GL088456.

Davis, J. M., Grindrod, P. M., Boazman, S. J., Vermeesch, P., Baird, T., (2020a), 'Quantified Aeolian Dune Changes on Mars Derived from Repeat Context Camera Images', Earth and Space Science, 0–3. https.//doi:10.1029/2019EA000874.

Ehlmann, B. L., Mustard, J.F., Swayze, G.A., Clark, R.N., Bishop, J.L., Poulet, F., Des Marais, D.J., Roach, L.H., et al. (2009), Identification of hydrated silicate minerals on Mars using MRO-CRISM: Geologic context near Nili Fossae and implications for aqueous alteration, Journal of Geophysical Research, 114, doi:10.1029/2009je003339.

Fenton, L. K., (2006), 'Dune migration and slip face advancement in the Rabe Crater dune field, Mars', Geophysical Research Letters, 33(20), L20201. https.//doi:10.1029/2006GL027133.

Fergason, R. L., Christensen, P. R., and Kieffer, H. H. (2006), 'High-resolution thermal inertia derived from the Thermal Emission Imaging System (THEMIS): Thermal model and applications', Journal of Geophysical Research E: Planets, 111(12), 1–22. https.//doi:10.1029/2006JE002735.

Flahaut, J., J. F. Mustard, C. Quantin, H. Clenet, P. Allemand, and P. Thomas (2011), Dikes of distinct composition intruded into Noachian-aged crust exposed in the walls of Valles Marineris, Geophysical Research Letters, 38(15), doi:10.1029/2011gl048109.

Frey, H. (1979), 'Thaumasia: A fossilized early forming tharsis uplift', Journal of Geophysical Research, 84(B3), 1009. https.//doi:10.1029/jb084ib03p01009.

Gao, X., Narteau, C., Rozier, O., and Courrech du Pont, S. (2015), 'Phase diagrams of dune shape and orientation depending on sand availability', Scientific Reports, 5. https.//doi:10.1038/srep14677.

Grindrod, P.M., Davis, J.M., Gupta, S., and Banham, S. (2019), 'Repeat Syn-Tectonic Sedimentation in Coprates Chasma, Mars' Paper presented at 50th Lunar and Planetary Science, Contribution 2132, Texas, United States.

Grindrod, P. M., Hollingsworth, J., Ayoub, F., and Hunt, S. A. (2018), 'The Search for Active Marsquakes Using Subpixel Coregistration and Correlation: Best Practice and First Results', Journal of Geophysical Research: Planets, 123(7), 1881–1900. https.//doi:10.1029/2018JE005649.

Herman, F., Anderson, B., and Leprince, S. (2011), 'Mountain glacier velocity variation during a retreat/advance cycle quantified using sub-pixel analysis of aster images', Journal of Glaciology, 57(202), 197–207. https.//doi:10.3189/002214311796405942.

Hollingsworth, J., Leprince, S., Ayoub, F., and Avouac, J-P. (2012), 'Deformation during the 1975-1984 Krafla rifting crisis, NE Iceland, measured from historical optical imagery', Journal of Geophysical Research: Solid Earth, 117(11), 1–24. https.//doi:10.1029/2012JB009140.

Jackson, D. W. T., Bourke, M. C., and Smyth, T. A. G. (2015), 'The dune effect on sand-transporting winds on Mars', Nature Communications. https.//doi:10.1038/ncomms9796.

Kirk, R. L., Howington-Kraus, E., Rosiek, M. R., Anderson, J. A., Archinal, B. A., Becker, K. J., Cook, D. A., et al. (2008), 'Ultrahigh resolution topographic mapping of Mars with MRO HiRISE stereo images : Meter-scale slopes of candidate Phoenix landing sites', 113, 1–31. https.//doi:10.1029/2007JE003000.

Lapotre, M. G. A., Ewing, R. C., Lamb, M. P., Fischer, W. W., Grotzinger, J. P., Rubin, D. M., Lewis, K. W., et al. (2016), 'Large wind ripples on Mars: A record of atmospheric evolution', Science. https.//doi:10.1126/science.aaf3206.

Leprince, S., Barbot, S., Ayoub, F., and Avouac, J-P. (2007), 'Automatic, Precise, Ortho-rectification and Coregistration for satellite Image Correlation, Application to Ground Deformation Measurement', IEEE J. Geosci. Rem. Sens., 45(6), 1529–1558. https.//doi:10.1109/TGRS.2006.888937.

Malin, M. C., Bell III, J. F., Cantor, B. A., Caplinger, M. A., Calvin, W. M., Todd Clancy, R., Edgett, K. S., et al. (2007), 'Context Camera Investigation on board the Mars Reconnaissance Orbiter', Journal of Geophysical Research E: Planets, 112(5), pp. 1–25. https.//doi:10.1029/2006JE002808.

Mandelbrot, B. B., and Wallis, J. R. (1968), 'Noah, Joseph , and operational hydrology', Water Resources Research, 4(5), pp. 909–918. https.//doi:10.1029/WR004i005p00909

McEwen, A. S., Eliason, E. M., Bergstrom, J. W., Bridges, N. T., Hansen, C. J., Delamere, A. W., Grant, J. A., et al. (2007), 'Mars reconnaissance orbiter's high resolution imaging science experiment (HiRISE)', Journal of Geophysical Research E: Planets, 112(5), 1–40. https.//doi:10.1029/2005JE002605.

Murchie, S., Arvidson, R., Bedini, P., Beisser, K., Bibring, J-P., Bishop, J., Boldt, J., et al. (2007), 'Compact Connaissance Imaging Spectrometer for Mars (CRISM) on Mars Reconnaissance Orbiter (MRO)', Journal of Geophysical Research E: Planets, 112(5), 1–57. https.//doi: 10.1029/2006JE002682.

Murchie, S. L., Seelos, F.P., Hash, C.d., Humm, D.C., Malaret, E., McGovern, J.A, Choo, T.H., et al. (2009), Compact Reconnaissance Imaging Spectrometer for Mars investigation and data set from the Mars Reconnaissance Orbiter's primary science phase, Journal of Geophysical Research: Planets, 114(E2), doi:10.1029/2009je003344.

Necsoiu, M., Leprince, S., Hooper, D. M., Dinwiddie, C. L., McGinnis, R. N., and Walter, G. R. (2009), 'Monitoring migration rates of an active subarctic dune field using optical imagery', Remote Sensing of Environment. https.//doi:10.1016/j.rse.2009.07.004.

Parente, M., H. D. Makarewicz, and J. L. Bishop (2011), Decomposition of mineral absorption bands using nonlinear least squares curve fitting: Application to Martian meteorites and CRISM data, Planetary and Space Science, 59(5), 423-442, doi:https://doi.org/10.1016/j.pss.2011.01.009.

Pelkey, S. M., Mustard, J.F., Murchie, S., Clancy, R.T., Wolff, M., Smith, M., Milliken, R., et al. (2007), CRISM multispectral summary products: Parameterizing mineral diversity on Mars from reflectance, Journal of Geophysical Research, 112(E8), doi:10.1029/2006je002831.

Reiss, D., Spiga, A., and Erkeling, G. (2014), 'The horizontal motion of dust devils on Mars derived from CRISM and CTX/HiRISE observations', Icarus. doi: 10.1016/j.icarus.2013.08.028.

Richardson, M. I., Toigo, A. D., and Newman, C. E. (2007), 'PlanetWRF: A general purpose, local to global numerical model for planetary atmospheric and climate dynamics', Journal of Geophysical Research E: Planets, 112(9), 1–29. https.//doi:10.1029/2006JE002825.

Runyon, K. D., Bridges, N. T., Ayoub, F., Newman, C. E., and Quade, J. J. (2017), 'An integrated model for dune morphology and sand fluxes on Mars', Earth and Planetary Science Letters. Elsevier, 457, 204–212. https.//doi:10.1016/J.EPSL.2016.09.054.

Sadler, P. (1981), 'Sediment Accumulation Rates and the Completeness of Stratigraphic Sections' The Journal of Geology, 89(5), 569–584. https.//doi:10.1086/628623

Sagan, C., Veverka, J., Fox, P., Dubisch, R., Lederberg, J., Levinthal, E., Quam, L., et al. (1972), 'Variable features on Mars: Preliminary mariner 9 television results', Icarus, 17(2), 346–372. https.//doi:10.1016/0019-1035(72)90005-X.

Seelos, F. P., Murchie, S. L., Humm, D. C., Barnouin, O. S., Morgan, F., Taylor, H. W., Hash, C., and Team C. (2011), CRISM Data Processing and Analysis Products Update — Calibration, Correction, and Visualization, in Lunar and Planetary Science Conference, edited, p. 1438.

Seelos, F. P., Viviano-Beck, C. E., Morgan, M. F., Romeo, G., Aiello, J. J., and Murchie S. L. (2016), CRISM Hyperspectral Targeted Observation PDS Product Sets — TERs and MTRDRs, in Lunar and Planetary Science Conference, edited, p. 1783.

Silvestro, S., Fenton, L. F., Vaz, D. A., Bridges, N. T., and Ori, G. G. (2010), 'Ripple migration and dune activity on Mars: Evidence for dynamic wind processes', Geophysical Research Letters. https.//doi:10.1029/2010GL044743.

Silvestro, S., Vaz, D. A., Yizhaq, H., and Esposito, F. (2016), 'Dune-like dynamic of Martian Aeolian large ripples', Geophysical Research Letters, 43(16), 8384–8389. https.//doi:10.1002/2016GL070014.

Skok, J. R., Mustard, J. F. Tornabene, L. L. Pan, C. Rogers, D., and Murchie, S. L., (2012), A spectroscopic analysis of Martian crater central peaks: Formation of the ancient crust, Journal of Geophysical Research: Planets, 117(E11), doi:10.1029/2012je004148.

Spiga, A. (2010), 'Martian mesoscale and microscale wind variability of relevance for dust lifting', The Mars Journal, 5, 146–158. https.//doi:10.1555/mars.2010.0006.

Spiga, A., and Forget, F. (2009), 'A new model to simulate the Martian mesoscale and microscale atmospheric circulation: Validation and first results', Journal of Geophysical Research E: Planets, 114(2), 1–26. https.//doi:10.1029/2008JE003242.

Sunshine, J. M., and Pieters C. M. (1993), Estimating modal abundances from the spectra of natural and laboratory pyroxene mixtures using the modified Gaussian model, Journal of Geophysical Research: Planets, 98(E5), 9075-9087, doi:10.1029/93je00677.

Tsoar, H. (1989), 'Linear dunes - forms and formation', Progress in Physical Geography, 13(4), pp. 507–528. https.//doi:10.1177/030913338901300402.

Vermeesch, P., and Drake, N. (2008), 'Remotely sensed dune celerity and sand flux measurements of the world's fastest barchans (Bodélé, Chad)', Geophysical Research Letters. https.//doi:10.1029/2008GL035921.

Viviano□Beck, C. E., Seelos, F.P., Murchie, S.L., Kahn, E.G., Seelos, K.D., Taylor, H.W., Taylor, K., et al. (2014), Revised CRISM spectral parameters and summary products based on the currently detected mineral diversity on Mars, Journal of Geophysical Research: Planets, 119(6), 1403-1431, doi:doi:10.1002/2014JE004627.